Signal Processing 178 (2021) 107793

Contents lists available at ScienceDirect

Signal Processing

journal homepage: www.elsevier.com/locate/sigpro

A novel fusion method based on dynamic threshold neural P systems and nonsubsampled contourlet transform for multi-modality medical images

Bo Li[a], Hong Peng[a,*], Jun Wang[b]

[a] School of Computer and Software Engineering, Xihua University, Chengdu, Sichuan, 610039, China
[b] School of Electrical Engineering and Electronic Information, Xihua University, Chengdu, 610039, China

ARTICLE INFO

Article history:
Received 13 February 2020
Revised 21 August 2020
Accepted 25 August 2020
Available online 7 September 2020

Keywords:
Dynamic threshold neural P systems
Nonsubsampled contourlet transform
Image fusion
Multi-modality medical images

ABSTRACT

Dynamic threshold neural P systems (DTNP systems) are a distributed parallel computing model with an interesting mechanism involving the cooperative spiking of neurons in a local region. In this paper, this mechanism is combined with the nonsubsampled contourlet transform (NSCT) to develop a novel fusion method for multi-modality medical images. The complementary information of multi-modality images is extracted using an improved novel sum-modified Laplacian (INSML) feature, which is used in the fusion rules for the low-frequency NSCT coefficients. Moreover, the high-frequency NSCT coefficients are extracted using the WLE-INSML features, which are used to construct the fusion rules for these coefficients. The proposed fusion method is evaluated on an open dataset consisting of twelve pairs of multi-modality medical images. In addition, it is compared with nine previously reported fusion methods and four deep learning based fusion methods. The qualitative and quantitative experimental results demonstrate the advantage of the proposed fusion method in terms of the visual quality and fusion performance.

1. Introduction

Multi-modality image fusion technology has emerged as a hot research topic in recent years [1,2] for multi-focus images and multi-modality medical images. Image fusion combines the complementary information from multi-modality sensors to enhance the visual perception of the human eyes or to mutually complement the limitations of each image. This technology has been applied in various fields such as visual surveillance, medicine, remote sensing and computer vision.

Multi-modality medical images are an important type of multi-modality images, where each constituent imaging modality has limitations and shows specific information. Magnetic resonance imaging (MRI) shows internal body structures such as the abdomen, liver, pancreas and other smooth tissues, while computed tomography (CT) highlights the bony structures and other anatomical parts with high resolution. Positron emission tomography (PET) and single-photon emission computed tomography (SPECT) images provide functional information related to metabolism. However, these images are often displayed in pseudo colour and typically have low resolution [3]. These multi-modality images can provide complementary information. To achieve higher diagnostic accuracy, many studies have combined the analysis of images obtained from different modalities of the same patient, which has led to the development of multi-modality medical image fusion techniques.

To merge two or more images from different modalities into a single fusion image, many fusion methods have been proposed in the past few years [4–8]. Multi-scale transform (MST)-based methods are a class of common fusion methods. However, compared with current state-of-the-art fusion methods, MST-based methods exhibit poor fusion performance. Due to this reason, several fusion techniques have been developed in recent years, such as sparse representation (SR) based fusion methods [9], image decomposition (ID) based fusion methods [10] and deep learning (DL) based fusion method [11].

1.1. Motivation and contribution

Dynamic threshold neural P (DTNP) systems are a recently developed distributed parallel neural-like computing model [12], incorporating the spiking mechanism and dynamic threshold mechanism. Our previous work demonstrated that DTNP systems are Turing-universal computing devices. This paper focuses on the application of DTNP systems to the fusion of multi-modality medical

* Corresponding author.
E-mail address: ph.xhu@hotmail.com (H. Peng).

https://doi.org/10.1016/j.sigpro.2020.107793
0165-1684/

images and proposes a novel DTNP system based fusion method in the NSCT domain.

The motivation behind this work is described as below.

(1) NSCT-based methods are early image fusion methods, which exhibit poor fusion performance compared with current state-of-the-art fusion methods, such as the SR-based and DL-based methods. However, the NSCT has some good characteristics that are conducive for image fusion, For example, the NSCT can retrieve the complementary information from multi-modality medical images.
(2) DTNP systems are a newly developed model and have an interesting characteristic, namely, the cooperative spiking of neurons in a local region. We sought to evaluate whether this characteristic could be combined with the NSCT to develop a novel fusion method for multi-modality medical images. Moreover, if the proposed fusion method can equal or even partially exceed the state-of-the-art fusion methods in terms of the fusion performance, this would demonstrate that some advantages of the DTNP systems could greatly improve the fusion performance of the NSCT-based methods for multi-modality medical images.

Due to the above reason, two DTNP systems are designed to present a novel fusion framework for multi-modality medical images. The proposed fusion framework consists of three parts: (i) the NSCT transform; (ii) image fusion in the NSCT domain; (iii) the inverse NSCT transform. The features of the high-frequency NSCT coefficients of the multi-modality medical images are regarded as the external inputs of the two DTNP systems, and their outputs are used as the control condition of the fusion rules.

The contributions of this paper can be summarized as follows:

(1) DTNP systems are used to design a novel fusion framework in the NSCT domain for multi-modality medical images, wherein the DTNP systems fully utilize the complementary information of the multi-modality medical images extracted by the NSCT.
(2) A fusion rule based on DTNP systems is developed, where the improved novel sum-modified Laplacian (INSML) features of the high-frequency NSCT coefficients of the multi-modality medical images are extracted and used as the external inputs of the DTNP systems, and the corresponding outputs are used to control the fusion rule. The INSML features can describe the detailed information, such as edges and contours, of multi-modality medical images better, and the INSML features in a local region can effectively trigger the cooperative spiking mechanism in DTNP systems.
(3) For the low-frequency NSCT coefficients, an INSML-WLE-based fusion rule is designed. It should be noted that the low-frequency NSCT coefficients not only express the main energy of an image, but also contain some detailed information. The WLE and INSML approaches are used for feature extraction to extract the main energy and detailed information of the multi-modality medical images, respectively. The two features are combined to control the fusion of the low-frequency NSCT coefficients.

In the study by Li et al. [13], DTNP systems were used to address the fusion of multi-focus images, where the combination of DTNP+ST+SF+SML was used to fuse the low- and high-frequency ST coefficients of the multi-focus images. While multi-focus images are retrieved by cameras using the same imaging principle but different focal lengths, multi-modality medical images are captured by devices using different imaging principles. However, the combination of DTNP+ST+SF+SML is not suitable for the fusion of multi-modality medical images. To achieve the ideal fusion effect, this work proposes the combination of DTNP+NSCT+WLE+INSML for the fusion of multi-modality medical images.

The rest of this paper is organized as follows. In Section 2, a review of the related literature is presented. Section 3 provides a detailed description of the proposed fusion framework in the NSCT domain for multi-modality medical images. In Section 4, the experimental results are detailed, while conclusions are drawn in Section 5.

2. Related work

In this section, we review various fusion methods for multi-modality images, including those proposed for multi-modality medical images.

2.1. MST-based fusion methods

Some of the early MST-based methods include the Laplacian pyramid (LP) [14], gradient pyramid [15], wavelet transform [16], discrete wavelet transform (DWT) [17] and dual-tree complex wavelet transform [18]. However, these methods suffer from drawbacks such as non-shift-invariance, poor spatiality and non-time-invariance. To overcome these drawbacks, several MST-based fusion methods have been introduced, including the curvelet transform [19], surfacelet transform [20], nonsubsampled shearlet transform (NSST) [21] and nonsubsampled contourlet transform (NSCT) [22].

Several fusion methods for multi-modality medical images have been developed in recent years. Singh and Khare [23] proposed a multi-modality medical image fusion method based on the Daubechies complex wavelet transform (DCWT), wherein the complex wavelet coefficients of the source images were fused based on the maximum selection rule. Manchanda et al. [24] proposed a method for multi-modality medical image fusion using the fuzzy transform. In a subsequent work, they presented an improved multi-modality medical image fusion method [25]. Singh and Anand [26] investigated a fusion method for multi-modality medical images, which used both the features retrieved by the discrete ripplet transform (DRT) and pulse coupled neural network. Padmavathi et al. [27] proposed an image fusion algorithm for constructing a fused image based on a total variation (TV-L1) model with an optimized adaptive weighting scheme. Yang et al. [28] developed a medical image fusion technique based on the multiscale geometric analysis of the contourlet transform.

2.2. SR-based fusion methods

SR-based fusion methods first identify the sparsest representation of the multi-modality images in a given dictionary before integrating the representation coefficients according to a fusion rule; then, the fused image is constructed by combining the given dictionary and fused sparse coefficients. In recent years, several SR-based fusion methods have been investigated [29–32]. However, only one dictionary is employed in the SR-based methods. To address this limitation, dictionary learning has been introduced in SR-based methods [33–35].

Concurrently, SR-based medical image fusion methods have received attention. Zhu et al. [36] proposed a dictionary learning based image fusion method, where image patches were obtained using a sampling scheme and classified by a clustering algorithm, and then, a dictionary was constructed using the K-SVD algorithm. Li et al. [37] reported a medical image fusion method based on discriminative low-rank sparse dictionary learning. Liu et al. [38] introduced a sparse representation model for pixel-level medical image fusion, termed convolutional sparsity based morphological

component analysis. Hu et al. [39] presented a medical image fusion method based on separable dictionary learning and Gabor filtering.

2.3. ID-based fusion methods

The key concept of ID-based fusion methods is based on the observation that natural images can be efficiently decomposed into morphological structure components, including texture and cartoon contents. To preserve the textural information, a new colour-gray image fusion algorithm based on morphological component analysis (MCA) was proposed to find the most important information [40]. To effectively exploit the morphological diversity property of the images and advantages of MCA, a novel multi-component fusion method was presented to generate improved fused images [41]. Maqsood and Javed [42] presented a multi-modal medical image fusion method based on two-scale image decomposition and sparse representation.

2.4. DL-based fusion methods

DL-based fusion methods are a class of attractive fusion methods as they achieve a competitive fusion performance. Recently, several DL-based fusion methods have been developed for the fusion of multi-modality images. Tang et al. [43] investigated a pixel convolutional neural network (CNN) for multi-focus image fusion, where a model was trained to learn the probabilities of the focused, defocused and unknown pixels based on their neighbourhood pixel information. Gao et al. [44] investigated a CNN for multi-focus image fusion where a deeper network was used for constructing an initial decision map. Amin-Naji et al. [45] presented a CNN-based multi-focus image fusion method combined with ensemble learning. In general, these fusion methods require a time-consuming training process compared with previous fusion methods.

For multi-modality image fusion, Li et al. [46] proposed a DL architecture, including encoder and decoder networks and termed this fusion method DenseFuse. Zhang et al. [47] presented a general multi-modality image fusion framework using CNNs, called IFCNN. These DL-based fusion methods have demonstrated a competitive fusion performance. Ma et al. [48] presented a dual-discriminator conditional generative adversarial network (DDcGAN) for the fusion of images with different resolutions. Li et al. [49] presented a multi-level image decomposition approach based on latent low-rank representation, called MDLatLRR.

3. The proposed fusion method

3.1. DTNP systems

DTNP systems [12] as a variant of spiking neural P systems (SNP systems) [50–55], are a type of distributed parallel computing models, which combine the spiking and dynamic threshold mechanisms of neurons. To implement the fusion of multi-modality medical images, DTNP systems are considered as a matrix of neurons with local connections.

Let I be a medical image with size $m \times n$ and $\mathrm{INSML}_{m\times n}$ is a feature matrix containing the (high-frequency) NSCT coefficients of the image. Therefore, a DTNP system Π is designed as a matrix of $m \times n$ neurons, as shown in Fig. 1, where the feature value INSML_{ij} is the external input of neuron σ_{ij}, and each neuron σ_{ij} has a local connect with the neurons in its r-neighbourhood $\delta_r(\sigma_{ij}) = \{\sigma_{kl} \mid |k-i| \le r,\ |l-j| \le r\},\ 1 \le i \le m, 1 \le j \le n$. Neuron σ_{ij} receives the spikes from the neighbouring neurons in δ_r, and then sends the generated spikes to its neighbouring neurons after applying the firing rule.

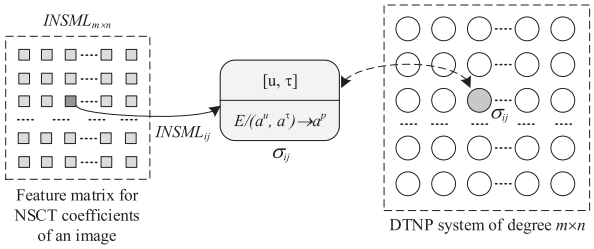

Fig. 1. A DTNP system Π and the corresponding feature matrix of NSCT coefficients, $V_{m\times n}$.

Neuron σ_{ij} has a data unit and dynamic threshold unit, $[u_{ij}, \tau_{ij}]$ and a spiking rule $E/(a^u, a^\tau) \to a^p$. Moreover, each neuron σ_{ij} is an input neuron, receiving an external input INSML_{ij} (i.e., INSML value of the (high-frequency) NSCT coefficient at position (i, j)), and it is also an output neuron.

For spiking rule $E/(a^u, a^\tau) \to a^p$ in neuron σ_{ij}, the firing condition E is defined as $E \equiv (u_{ij}(t) \ge \tau_{ij}(t)) \wedge (u_{ij}(t) \ge u) \wedge (\tau_{ij}(t) \ge \tau)$. If the firing condition is satisfied, then neuron σ_{ij} fires, indicating that the spikes with value u in the data unit and the threshold with value τ in the dynamic threshold unit are consumed, and then, the spikes with value p are produced and sent to the neighbouring neurons. Based on the spiking mechanism, the state equation for neuron σ_{ij} can be defined as

$$u_{ij}(t+1) = \begin{cases} u_{ij}(t) - u + V_{ij} + \sum\limits_{\sigma_{kl}\in\delta_r} w_{kl}p_{kl}(t), & \text{if } \sigma_{ij} \text{ fires} \\ u_{ij}(t) + V_{ij} + \sum\limits_{\sigma_{kl}\in\delta_r} w_{kl}p_{kl}(t), & \text{otherwise} \end{cases} \quad (1)$$

$$\tau_{ij}(t+1) = \begin{cases} \tau_{ij}(t) - \tau + p, & \text{if } \sigma_{ij} \text{ fires} \\ \tau_{ij}(t), & \text{otherwise} \end{cases} \quad (2)$$

where $p_{kl}(t)$ is the value of the spikes received by neuron σ_{ij} from the neighbouring neuron σ_{kl} and $w_{kl}(t)$ is the corresponding local weight, and V_{ij}=INSML_{ij} is an external stimulus; p is the value of the spikes produced by σ_{ij} when it fires.

The working procedure for the DTNP system Π can be described as follows. Initially, for each neuron σ_{ij}, we set $u_{ij}(0) = v_{ij}(0) = 0$ and $\tau_{ij}(0) = \tau_0$, and assign $W_{r\times r}$. DTNP system Π starts from the initial state and an external input matrix $\mathrm{INSML}_{m\times n}$, and is then executed iteratively until iteration number $t_{\max}$ is reached. The system then halts. During the computation, the sum of spikes that each neuron σ_{ij} sends is considered as its output and used as a control signal for the fusion of the multi-modality medical images. For simplicity, a maximum consumption strategy is adopted when applying the firing rules (i.e., set $u = u_{ij}(t)$ and $\tau = \tau_{ij}(t)$).

The working procedure for the DTNP system Π can be described as follows. Initially, for each neuron σ_{ij}, we set $u_{ij}(0) = v_{ij}(0) = 0$ and $\tau_{ij}(0) = \tau_0$, and assign $W_{r\times r}$. DTNP system Π starts from the initial state and an external input matrix $\mathrm{INSML}_{m\times n}$, and is then executed iteratively until iteration number $t_{\max}$ is reached. The system then halts. During the computation, the sum of spikes that each neuron σ_{ij} sends is considered as its output and used as a control signal for the fusion of the multi-modality medical images. For simplicity, a maximum consumption strategy is adopted when applying the firing rules (i.e., set $u = u_{ij}(t)$ and $\tau = \tau_{ij}(t)$).

Based on the working procedure, a DTNP system Π is implemented in Algorithm 1. It should be noted that $W = (w_{ij})_{r\times r}$ is a local weight matrix; $T = (\tau_{ij})_{m\times n}$ is a threshold matrix; $U = (u_{ij})_{m\times n}$ is a data (or state) matrix; $P = (P_{ij})_{m\times n}$ is a spike sum matrix that accumulates the generated spikes when neuron σ_{ij} fires; τ_0 is the initial threshold; p is the initial value of the generated spikes; r is the neighbourhood radius. The input of Algorithm 1 is

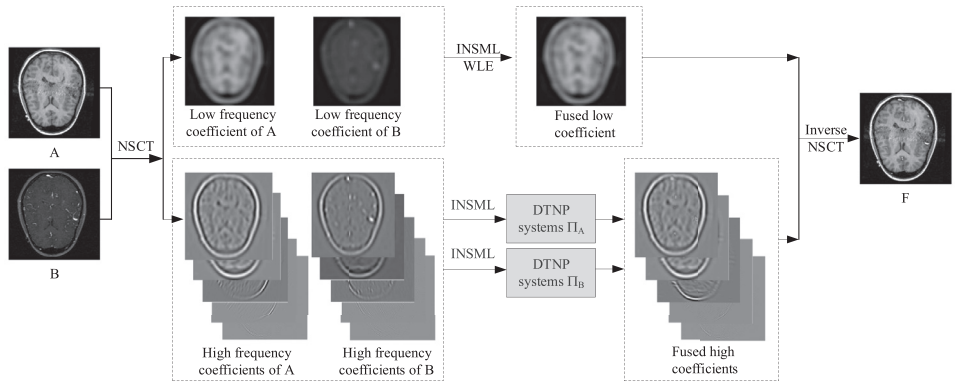

Fig. 2. Proposed fusion framework based on DTNP systems in the NSCT domain, where the two source images are multi-modality medical images.

Algorithm 1 DTNP systems. Call format: P=DTNP(V)

Input:
INSML feature matrix, $V = (V_{ij})_{m\times n}$;
Output:
Spike sum matrix, $P = (P_{ij})_{m\times n}$;
Assign priori parameters: $t_{\max}$, τ_0, p, r, $W = (w_{ij})_{r\times r}$;
/* Initialization */
$U = (u_{ij})_{m\times n} = (0)_{m\times n}$;
$T = (\tau_{ij})_{m\times n} = (\tau_0)_{m\times n}$;
$P = (P_{ij})_{m\times n} = (0)_{m\times n}$;
/* Working procedure of DTNP systems */
for each $t \in [1, t_{\max}]$ **do**
  for each $i \in [1, m]$ **do**
    for each $j \in [1, n]$ **do**
      Update u_{ij} in U using Eq.~(2);
      Update τ_{ij} in T using Eq.~(3);
      if $u_{ij} \geq \tau_{ij}$ **then**
        $P_{ij} = P_{ij} + p$;
      end if
    end for
  end for
end for
/* Output */
return P;

an INSML feature matrix of NSCT coefficients, $V = (V_{ij})_{m\times n}$, and its output is a spike sum matrix, $P = (P_{ij})_{m\times n}$.

3.2. Image fusion framework for multi-modality medical images

We propose a DTNP -system based image fusion framework in the NSCT domain for multi-modality medical images, as shown in Fig. 2. The proposed fusion framework includes three parts, namely (i) the NSCT transform, (ii) fusion rules and (iii) the inverse NSCT transform. In Fig. 2, the two source images are multi-modality medical images.

The multi-modality medical images are decomposed into NSCT coefficients using the NSCT transform. Then, the NSCT coefficients are fused to generate the fused NSCT coefficients. However, the low-frequency and high-frequency coefficients are merged separately using distinct fusion rules. The high-frequency NSCT coefficients are fused using a DTNP system based fusion rule, while the low-frequency NSCT coefficients adopt an INSML-WLE rule. The DTNP systems are a key component of the proposed fusion framework and have been designed to control the fusion of the high-frequency NSCT coefficients. Two DTNP systems, Π_A and Π_B, are considered for merging the high-frequency coefficients of two multi-modality medical images, A and B, respectively. The fused NSCT coefficients are converted to reconstruct a fusion image using the inverse NSCT transform.

Therefore, based on the fusion framework, the proposed fusion method for multi-modality medical images involves the following steps:

(i) NSCT transform: The multi-modality medical images are decomposed into NSCT coefficients using the NSCT transform. Thus, low- and high-frequency NSCT coefficients are obtained for each of the multi-modality medical images being evaluated.
(ii) Fusion of low-frequency NSCT coefficients: The low-frequency NSCT coefficients of the multi-modality medical images are fused using INSML-WLE (Eq. (6)).
(iii) Fusion of high-frequency NSCT coefficients: The INSML feature matrices of the high-frequency NSCT coefficients of the multi-modality medical images are regarded as the external inputs of the DTNP systems Π_A and Π_B. The two DTNP systems start from the initial state and are then executed continuously until the iteration number $t_{\max}$ is reached. Subsequently, they halt. The outputs of the two DTNP systems are then used as the control signal of the high-frequency fusion rules (Eq. (7)).
(iv) Inverse NSCT transform: The combined NSCT coefficients are converted back to reconstruct the fusion image using the inverse transform.

In the following subsections, the two fusion rules used for the low-frequency and high-frequency NSCT coefficients are explained in detail.

3.2.1. Fusion rules for low-frequency NSCT coefficients

In general, the fusion strategy adopted for the low-frequency coefficients has a significant impact on the final fusion image. In the proposed fusion method, two important factors, namely, energy preservation and detail extraction, are considered. As it is well established, most of the energy of an image is contained in its low-frequency coefficients, and the energy strengths of different source images at the same position might have a larger difference, as the source images are obtained via different medical imaging mechanisms. Therefore, the commonly used 'weighted-averaging' based fusion rules can often result in energy loss in the fused medical image. Consequently, the brightness can drop sharply leading to poor visual effects. To overcome this limitation, an activity level measure, called WLE, is introduced for the low-frequency coefficients. The WLE features are computed based on the low-frequency coefficients in a local neighbourhood, which are used to express most of the energy of a medical image.

WLE is defined as

$$\mathrm{WLE}_{l0}(i,j)=\sum_a\sum_b W'(a,b)C_{l0}(i+a,j+b)^2 \tag{3}$$

where $C_{l0}(i,j)$ is the low-frequency NSCT coefficient at position (i,j), and W' is a weight matrix that is defined as

$$W'=\frac{1}{16}\begin{vmatrix}1&2&1\\2&4&2\\1&2&1\end{vmatrix}$$

.

Usually, the low-frequency coefficients can also contain a small amount of detailed information, which is useful for the fusion of multi-modality medical images. To extract the detailed information, an INSML is considered. The INSML feature is defined as follows:

$$\mathrm{INSML}_{l0}(i,j)=\sum_a\sum_b W''(a,b)\mathrm{IML}_{l0}(i+a,j+b) \tag{4}$$

where W'' is a weight matrix that is defined as

$$W''=\frac{1}{15}\begin{vmatrix}1&2&1\\2&3&2\\1&2&1\end{vmatrix}$$

and IML is given by

$$\begin{aligned}\mathrm{IML}_{l0}(i,j)&=|2C_{l0}(i,j)-C_{l0}(i-1,j)-C_{l0}(i+1,j)|\\&+|2C_{l0}(i,j)-C_{l0}(i,j-1)-C_{l0}(i,j+1)|\\&+\frac{1}{\sqrt{2}}|2C_{l0}(i,j)-C_{l0}(i-1,j-1)-C_{l0}(i+1,j+1)|\\&+\frac{1}{\sqrt{2}}|2C_{l0}(i,j)-C_{l0}(i-1,j+1)-C_{l0}(i+1,j-1)|.\end{aligned} \tag{5}$$

where $C_{l0}(i,j)$ is the low-frequency coefficient at position (i,j). It should be noted that the diagonal coefficients and adjacent information are considered in $\mathrm{IML}_{l0}(i,j)$, and a factor $\frac{1}{\sqrt{2}}$ is set for the diagonal coefficients.

The INSML and WLE features express the main energy and partial details of the multi-modality medical images, respectively. Thus, a combination of WLE and INSML, called the WLE-INSML feature, is used to develop a fusion rule for the low-frequency coefficients of the multi-modality medical images. Suppose $\alpha^A_{l0}(i,j)=\mathrm{INSML}^A_{l0}(i,j)\times\mathrm{WLE}^A_{l0}(i,j)$ and $\alpha^B_{l0}(i,j)=\mathrm{WLE}^B_{l0}(i,j)\times\mathrm{INSML}^B_{l0}(i,j)$, which are associated with the source images A and B. Based on the WLE-INSML features, the fusion rules for the low-frequency coefficients can be defined as:

$$C^F_{l0}(i,j)=\begin{cases}C^A_{l0}(i,j), & \text{if } \alpha^A_{l0}(i,j)\geq\alpha^B_{l0}(i,j)\\ C^B_{l0}(i,j), & \text{otherwise}\end{cases} \tag{6}$$

where $C^A_{l0}(i,j)$ and $C^B_{l0}(i,j)$ are the low-frequency NSCT coefficients of the two multi-modality medical images at position (i,j), and $C^F_{l0}(i,j)$ are the low-frequency coefficients of the fusion image F at position (i,j).

The fusion rule for the low-frequency NSCT coefficients is implemented in Algorithm 2.

Algorithm 2 Fusion of low-frequency NSCT coefficients. Call format: $C^F_0=\mathrm{LowFrequncyFusion}\,(C^A_0,C^B_0)$

Input:
Low-frequency NSCT coefficients of image I_A, $C^A_0=(C^A_0(i,j))$;
Low-frequency NSCT coefficients of image I_B, $C^B_0=(C^B_0(i,j))$;
Output:
Fused low-frequency NSCT coefficients, $C^F_0=(C^F_0(i,j))$;

```
for each i ∈ [1, m] do
  for each j ∈ [1, n] do
    Compute WLE^A_l0(i,j) and WLE^B_l0(i,j) based on Eq.~(3);
    Compute INSML^A_l0(i,j) and INSML^B_l0(i,j) based on Eq.~(4);
    α^A_l0(i,j) = INSML^A_l0(i,j) × WLE^A_l0(i,j);
    α^B_l0(i,j) = INSML^B_l0(i,j) × WLE^B_l0(i,j);
    if α^A_l0(i,j) ≥ α^B_l0(i,j) then
      C^F_0(i,j) = C^A_0(i,j);
    else
      C^F_0(i,j) = C^B_0(i,j);
    end if
  end for
end for
return C^F_0;
```

3.2.2. Fusion rules for high-frequency NSCT coefficients

The high-frequency coefficients contain the edges and contours of an image, and they represent the richness of the information at the corresponding location. In the NSCT decomposition, a coefficient with a large absolute value corresponds to a pixel where the brightness changes suddenly, i.e., edge features with a larger contrast in the image, such as the boundary, bright line and outline of a region. When the absolute value of the high-frequency coefficient is larger, rich detailed information can often be obtained. To generate the high-frequency fusion image with rich detailed information, the INSML features of the high-frequency coefficients are adopted to express the edge features of an image, denoted by $\mathrm{INSML}_{l_r}(i,j)$. The INSML features are used as the external inputs of the DTNP systems, which have an interesting characteristic, namely, the cooperative firing of adjacent neurons. The INSML features are computed based on the adjacent high-frequency coefficients in a local neighbourhood. Therefore, the INSML features of adjacent high-frequency coefficients can trigger adjacent neurons.

Let Π_A and Π_B be two DTNP systems, which are associated with the source multi-modality medical images, A and B. The features of the high-frequency coefficients of the multi-modality medical images, respectively, are regarded as the external inputs of Π_A and Π_B. Starting from the initial state, the two DTNP systems continuously execute until the iteration number $t_{\max}$ is reached. Then, the execution halts. Let P_A and P_B denote the spiking sum matrices associated with Π_A and Π_B, respectively, i.e., $P_A=(p^A_{ij})_{m\times n}$ and $P_B=(p^B_{ij})_{m\times n}$, where p^A_{ij} (resp. p^B_{ij}) is the cumulative value of the spikes sent by neuron σ_{ij} in Π_A (resp. Π_B). Based on the two spiking matrices, the fusion rules of the high-frequency NSCT coefficients can be defined as follows:

$$C^F_{l_r}(i,j)=\begin{cases}C^A_{l_r}(i,j), & \text{if } p^A_{ij}\geq p^B_{ij}\\ C^B_{l_r}(i,j), & \text{if } p^A_{ij}<p^B_{ij}\end{cases} \tag{7}$$

where $C^A_{l_r}(i,j)$ and $C^B_{l_r}(i,j)$ are the high-frequency coefficients of the multi-modality medical images in layer l, direction r and position (i,j), and $C^F_{l_r}(i,j)$ are the high-frequency coefficients of the fused image F in layer l, direction r and position (i,j), for $1\leq i\leq m$ and $1\leq j\leq n$.

Fig. 3 illustrates an example of the activity levels of the outputs P_A and P_B of the DTNP systems Π_A and Π_B, respectively, on the high-frequency coefficient planes for a pair of CT and MRI images. The NSCT transform has 22 high-frequency coefficient planes under the parameters '[1 2 3 3]'. The activity images are binary images, where the white dot indicates that P_A has a higher activity level than P_B and vice versa. It can be observed that these activity images are different for the 22 high-frequency coefficient planes.

The fusion rule for the high-frequency NSCT coefficients is implemented in Algorithm 3. In Algorithm 3, N denotes the number of high-frequency decomposition planes for all layers and directions.

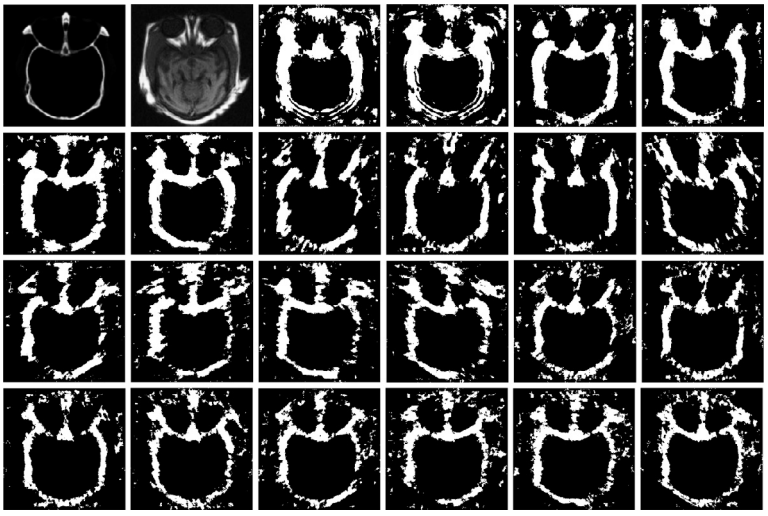

Fig. 3. Activity levels of outputs P_A and P_B of the DTNP systems Π_A and Π_B on the high-frequency coefficient planes. The first two images correspond to the source CT and MRI images, and the other images represent the activity level images of the corresponding 22 high-frequency coefficient planes.

Algorithm 3 Fusion of high-frequency NSCT coefficients. Call format: C_l^F = HighFrequncyFusion (C_l^A, C_l^B).

Input:
High-frequency NSCT coefficients of image I_A: $C_l^A = (C_l^A(i,j))$;
High-frequency NSCT coefficients of image I_B: $C_l^B = (C_l^B(i,j))$;
Output:
Fused high-frequency NSCT coefficients: $C_l^F = (C_l^F(i,j))$;
/* Compute the INSML feature matrixes of C_l^A and C_l^B: $V_A = (V_{ij}^A)$ and $V_B = (V_{ij}^B)$ */
for each $i \in [1, m]$ **do**
  for each $j \in [1, n]$ **do**
    Compute $V_{ij}^A = \mathrm{INSML}_{l}^{A}(i,j)$ of C_l^A based on Eq.~(4);
    Compute $V_{ij}^B = \mathrm{INSML}_{l}^{B}(i,j)$ of C_l^B based on Eq.~(4);
  end for
end for
/* Compute the spike sum matrices of V_A and V_B: $P_A = (P_{ij}^A)$ and $P_B = (P_{ij}^B)$ */
P_A=DTNP(V_A);
P_B=DTNP(V_B);
for each $i \in [1, m]$ **do**
  for each $j \in [1, n]$ **do**
    if $P_{ij}^A \geq P_{ij}^B$ **then**
      $C_l^F(i,j) = C_l^A(i,j)$;
    else
      $C_l^F(i,j) = C_l^B(i,j)$;
    end if
  end for
end for
return C_l^F;

3.3. Implementation of the proposed fusion method

The proposed fusion method is based on DTNP systems in the NSCT domain for the fusion of multi-modality medical images. According to the image fusion framework shown in Fig. 2 and the steps detailed above, the proposed fusion method is implemented in Algorithm 4. Algorithm 4 has two inputs, images I_A and I_B and one output, i.e., the fused image I_F. In Algorithm 4, NSCT(·) represents a NSCT transformation, and INSCT(·) is the corresponding inverse NSCT transformation; C_0^A (resp. C_0^B) is the matrix of low-frequency coefficients of image I_A (resp. I_B), and C_l^A (resp. C_l^B) is the matrix of high-frequency coefficients of image I_A (resp. I_B), for $1 \leq l \leq N$, where N is the number of high-frequency decomposition planes.

Algorithm 4 Proposed fusion algorithm for multi-modality medical images.

Input:
Multi-modality medical images, I_A and I_B;
Output:
Fused image I_F;
/* NSCT decomposition of image I_A */
1: $[C_0^A, C_1^A, \cdots, C_N^A]$=NSCT($I_A$);
/* NSCT decomposition of image I_B */
2: $[C_0^B, C_1^B, \cdots, C_N^B]$=NSCT($I_B$);
/* fusion of low-frequency coefficients */
3: C_0^F=LowFrequncyFusion(C_0^A, C_0^B);
/* fusion of high-frequency coefficients */
4: **for** each $l \in [1, N]$ **do**
5: C_l^F=HighFrequncyFusion(C_l^A, C_l^B);
6: **end for**
/* Inverse NSCT transform */
7: I_F=INSCT($C_0^F, C_1^F, \cdots, C_N^F$);
8: **return** I_F;

4. Experimental results

To evaluate the effectiveness of the proposed fusion method, twelve pairs of multi-modality medical images were evaluated in the experiments, as shown in Fig. 4, including MRI_T1 and MRI_T2, CT and MRI, MRI and PET, MRI and SPECT images. These images with a size of 256 × 256 were downloaded from the open source database "http://www.med.harvard.edu/aanlib/ ".

In the experiments, the proposed fusion method was compared with nine methods, including the Wavelet [16], DWT [56], CVT [19], DTCWT [18], ASR [57], NSCT [22], NSCT-SR [58], NSCT-SF-PCNN [59], NSST-PAPCNN[60] and four fusion methods based on DL DenseFuse [46], IFCNN [47], DDcGAN [48] and MDLatLRR [49]).

The proposed fusion method is a DTNP system based fusion method in the NSCT domain. The NSCT employs a pyramid filter and directional filter with the parameters "PKVA", "9/7" and "[1 2 3 3]". The parameters of the DTNP systems were set to $t_{\max} = 110$,

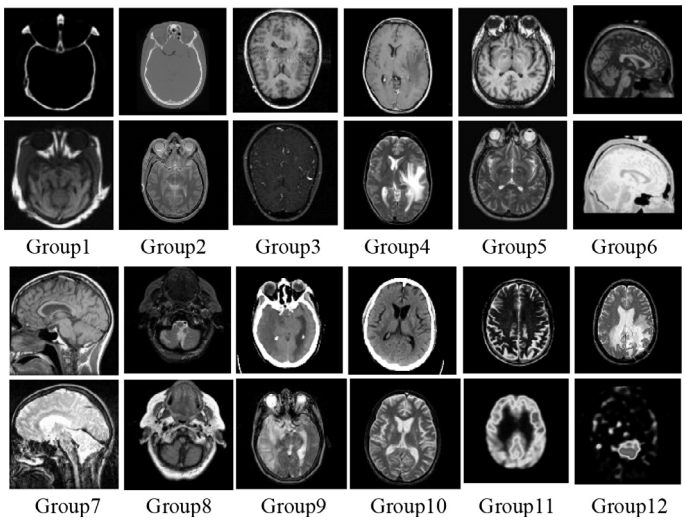

Fig. 4. Medical image dataset containing twelve pairs of multi-modality medical images.

$\tau_0 = 1,\ \tau = 1,\ r = 3$ and $p = 1.1$. In addition, $W_{3\times3} = \{w_{ij}\}_{3\times3}$ is determined as follows: (i) $w_{22} = 0$; (ii) $w_{ij} = 1/sqrt((i-2)^2 + (j-2)^2)$ for $i \neq 2, j \neq 2, 1 \leq i \leq 3, 1 \leq j \leq 3$.

The proposed fusion method was implemented in Matlab 2017b on an Intel Core i7-6700 3.4GHz CPU with 16GB RAM. Except for the four fusion methods based on DL, all other compared methods were also implemented on the same platform using open source codes or codes provided by the authors cited in this paper. The IFCNN, DenseFuse, DDcGAN and MDLatLRR networks were implemented on an Ubuntu 16.04 OS and Inter Xeno Silver 4110 2.10GHz CPU and NVIDIA Tesla P100 with 16GB RAM using the open source codes provided by the respective authors.

In the experiments, six fusion quality metrics were adopted to objectively evaluate the proposed and compared fusion methods, including Petrovics metric (Qabf) [61], mutual information (MI) [62], feature mutual information (FMI) [63], sum of the correlations of differences (SCD) [64], structural similarity index measure (MS_SSIM) [65] and standard deviation (SD) [66]. For the six metrics, the larger the metric value, the better the fusion performance of the corresponding method.

In the first group of experiments, the proposed method was compared with nine previous fusion methods, including the Wavelet, DWT, CVT, DTCWT, ASR, NSCT, NSCT-SR, NSCT-SF-PCNN and NSST-PAPCNN. Two pairs of medical images with different types in the dataset have been used to show the experimental results, i.e., 'Group 1' and 'Group 6', which have different types of medical images, namely CT/MRI and MRI_T1/MRI_T2. The images fused with these methods are shown in Figs. 5 and 6. It can be observed from Fig. 5 that: (1) The image fused with the Wavelet does not retain the detailed information of the source images well and has an overall low brightness; (2) Some blurring exists in the image fused using the DWT, leading to an undesirable fusion result; (3) The above problem can also be observed in the fusion images obtained with the CVT, DTCWT, ASR, NSCT and NSCT-SF-PCNN, which exhibit lower contrast and brightness. In contrast, the images fused using the proposed method, NSCT-SR and NSST-PAPCNN not only retain the detailed information of the source images but also exhibit high contrast. To better distinguish the differences between the fused images, an enlarged view of the detail in the local area shown in Figures (i), (k) and (l) is presented. It can be observed from the enlarged boxes that the proposed method fuses more detailed information from the multi-modality images, while the images fused with the NSCT-SR and NSST-PAPCNN have relatively fewer details.

It can be observed from Fig. 6 that (1) For the MRI-type medical images, the image fused with the DWT is blurred to a certain extent. (2) The Wavelet does not preserve the details of the source images better; (3) The images fused with the Wavelet, DWT, CVT, DTCWT, ASR and NSCT have a lower contrast and brightness. (4)?The images fused with the NSCT-SR and NSCT-SF-PCNN contain more shadows. However, the proposed method and NSST-PAPCNN can preserve the detailed information of the source images and

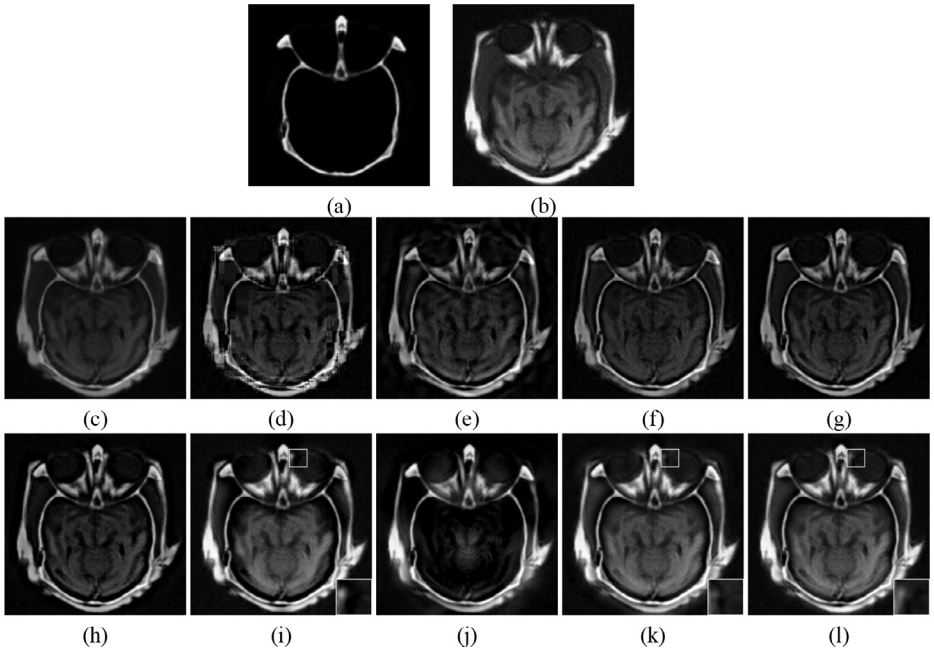

Fig. 5. Fusion results obtained for the 'Group 1' images: (a) source CT image, (b) source MRI image, (c) Wavelet, (d) DWT, (e) CVT, (f) DTCWT, (g) ASR, (h) NSCT, (i) NSCT-SR, (j) NSCT-SF-PCNN, (k) NSST-PAPCNN and (l) the proposed method.

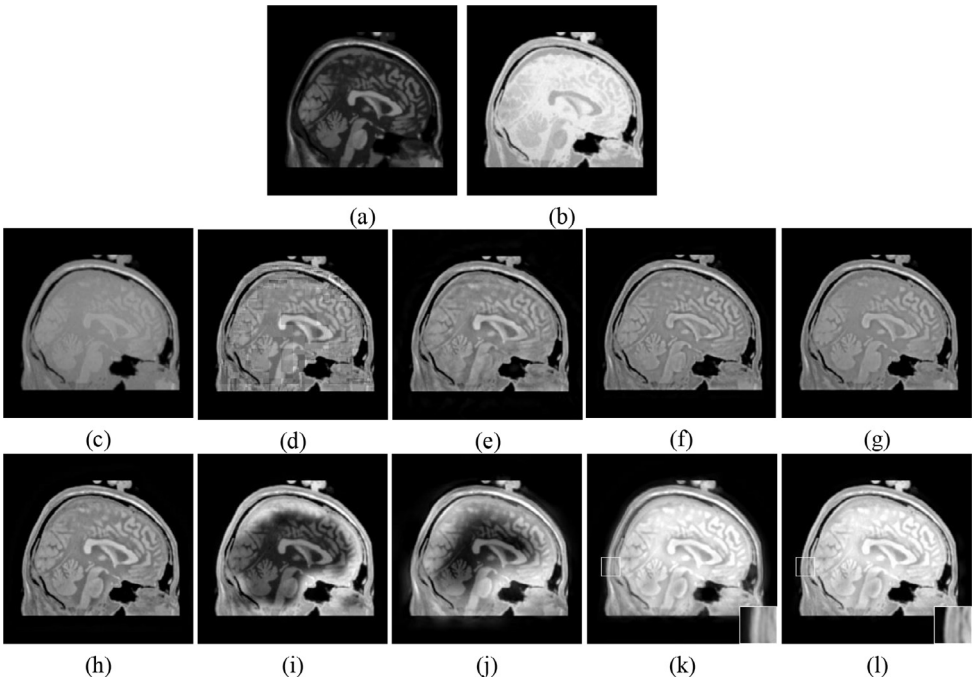

Fig. 6. Fusion results obtained for the 'Group 6' images: (a) source MRI_T1 image, (b) source MRI_T2 image, (c) Wavelet, (d) DWT, (e) CVT, (f) DTCWT, (g) ASR, (h) NSCT, (i) NSCT-SR, (j) NSCT-SF-PCNN, (k) NSST-PAPCNN and (l) the proposed method.

Table 1
Comparison between the results of the proposed method and previous methods evaluated on two pairs of multi-modality medical images in terms of six metrics.

Images	Method	Qabf	MI	FMI	SCD	MS_SSIM	SD
Group 1 CT/MR1	Wavelet	0.4038	11.8110	0.9019	1.3350	0.8638	33.5205
	DWT	0.5570	12.2950	0.8766	1.4341	0.8543	45.4366
	CVT	0.5593	12.5179	0.8961	1.4118	0.8445	41.2239
	DTCWT	0.6041	12.5481	0.9038	1.4386	0.8965	37.7423
	ASR	0.7068	12.3557	0.9028	1.5144	0.9355	40.0486
	NSCT	0.7087	12.2556	0.9050	1.6033	0.9465	45.0023
	NSCT-SR	0.7254	13.1784	0.9056	1.6626	0.9377	**56.8796**
	NSCT-SF-PCNN	0.5782	11.8549	**0.9090**	1.4566	0.8214	53.4049
	NSST-PAPCNN	0.6873	**13.9104**	0.9016	1.7223	0.9249	56.0239
	Proposed	**0.7371**	13.6377	0.9047	**1.7269**	**0.9478**	55.9198
Group 6 MR1_T1/ MR2_T2	Wavelet	0.4197	8.6867	0.8949	0.4425	0.8318	65.3143
	DWT	0.5269	8.8097	0.8803	0.4904	0.8364	69.6428
	CVT	0.5309	10.4741	0.8898	0.4723	0.8608	67.5608
	DTCWT	0.5384	9.5217	0.8943	0.4526	?0.8637	66.6649
	ASR	0.5586	8.4815?	0.8940	0.4663	0.8786	67.2142
	NSCT	**0.5905**	9.9105	0.8902	0.5404	**0.8877**	68.5398
	NSCT-SR	0.5885	10.4861	0.9036	0.1723	0.7951	72.5683
	NSCT-SF-PCNN	0.5393	**12.1960**	0.8952	0.3262	0.7613	75.2603
	NSST-PAPCNN	0.5016	11.5344	0.8819	1.1824	0.8271	98.0668
	Proposed	0.5801	10.4887	**0.9039**	**1.3197**	0.8716	**100.2606**

achieve high contrast. It can be observed from the enlarged boxes that the proposed method fuses more detailed information from the multimodality images compared with NSST-PAPCNN.

As it is difficult to judge the quality of the images fused with these methods based on subjective visual effects, an objective assessment is necessary. Table 1 shows a quantitative comparison of ten fusion methods for the two pairs of medical images in terms of six metrics. In Table 1, the numerical values in bold font indicate that the corresponding method achieved the best metric value. For "Group 1" (CT/MRI images), it can be observed from Table 1 that: (i) the proposed fusion method achieves the best value in terms of three metrics, namely the Qabf, SCD and MS_SSIM; (ii) the proposed fusion method achieves the next-best value in terms of the MI; (iii) the proposed fusion method achieves high values in terms of the FMI and SD.

For "Group 6" (MRI_T1/MRI_T2 images), it can be observed from Table 1 that: (i) the proposed fusion method achieves the best value in terms of three metrics, namely the FMI, SCD and SD; (ii) the proposed fusion method achieves a high value in terms of the Qabf, MI and MS_SSIM.

The average fusion performance of the proposed method and nine previous methods on the entire dataset in terms of six metrics is also presented, as shown in Table 2. It can be observed from Table 2 that: (i) the proposed fusion method achieves the best value in terms of three metrics, namely the FMI, SCD and SD; (ii) the proposed fusion method achieves the next-best value in

Table 2
Comparison between the results of the proposed method and previous methods for the dataset in terms of six metrics.

Images	Method	Qabf	MI	FMI	SCD	MS_SSIM	SD
Dataset	Wavelet	0.3897	10.0751	0.8690	0.8521	0.8705	53.6580
	DWT	0.5079	10.3557	0.8625	0.8765	0.8749	61.7084
	CVT	0.5135	**11.5817**	0.8699	0.8802	0.8817	59.2285
	DTCWT	0.5361	10.7497	0.8748	0.8815	0.8960	57.0032
	ASR	0.5784	10.1581	0.8785	0.9105	0.9086	57.4626
	NSCT	0.5798	10.7822	0.8763	0.9753	**0.9369**	60.8543
	NSCT-SR	**0.6033**	11.0311	0.8704	1.1197	0.9265	69.4709
	NSCT-SF-PCNN	0.5335	11.1061	0.8741	1.0384	0.8642	69.3907
	NSST-PAPCNN	0.5530	11.5741	0.8726	1.4069	0.9224	75.0621
	Proposed	0.5805	11.3653	**0.8787**	**1.4144**	0.9324	**75.1189**

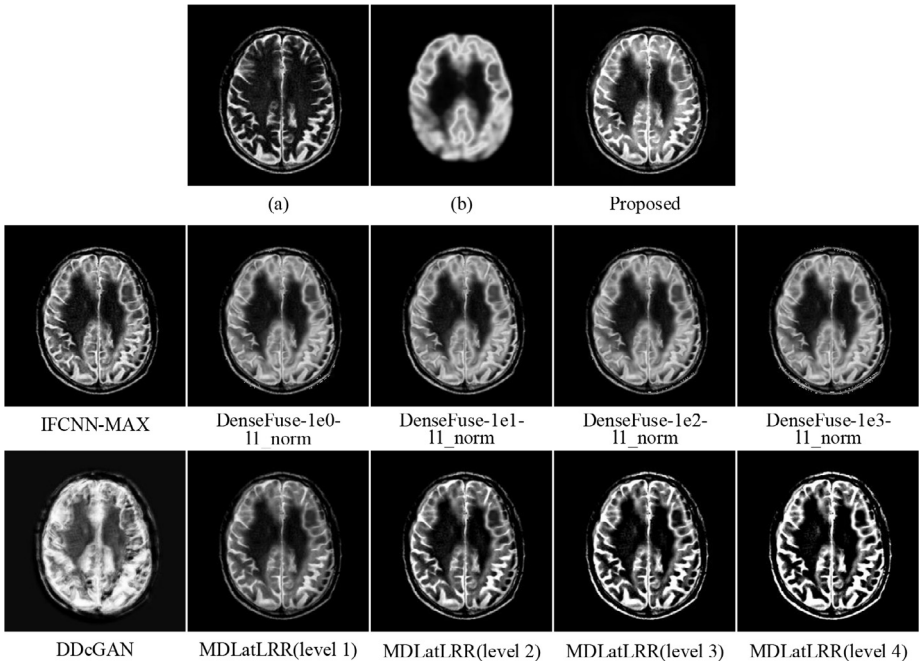

Fig. 7. Fusion results on the 'Group 11' images: (a) source MRI image and (b) source PET image.

terms of the Qabf and MS_SSIM; (iii) the proposed fusion method achieves a high value in terms of the MI.

Recently, image fusion methods based on DL have been developed, which have shown good fusion performance. The proposed method was compared with four methods based on DL, namely IFCNN [47], DenseFuse [46], DDcGAN [48] and MDLatLRR [49]. Two pairs of typical multi-modality medical images were used in the experiments, termed "Group 11" (MRI/PET) and "Group 12" (MRI/SPECT). Fig. 7 and Fig. 8 show the images fused using the proposed method and four methods based on DL on the two pairs of medical images, where (a) and (b) correspond to the two source medical images from different modalities.

For the MRI/PET images shown in Fig. 7, the proposed method, MDLatLRR, IFCNN and DenseFuse show good fusion performance visually; however, DDcGAN appears a little blurry. In Fig. 8, it can be observed that both the proposed method and MDLatLRR (level 3 and level 4) retain more details and have better contrast compared with the other methods. However, we cannot visually judge which method is the best or worst among the three fusion methods.

Table 3 presents a quantitative comparison between the results of the presented method and four methods based on DL for two pairs of medical images in terms of six metrics. The numerical values in bold correspond to the method that achieves the best value for each metric. For "Group 11" (MRI/SPECT images), it can be observed from Table 3 that: (i) the proposed fusion method achieves the best value in terms of two metrics, namely the FMI and SCD; (ii) the proposed fusion method achieves the next-best value in terms of the Qabf and MI; (iii) the proposed fusion method achieves a high value in terms of the MS_SSIM and SD.

For "Group 12" (MRI/PET images), it can be observed from Table 3 that: (i) the proposed fusion method achieves the best value in terms of three metrics, namely the Qabf, FMI and SCD; (ii) the proposed fusion method achieves the next-best value of MS_SSIM=0.9607.

We present the average fusion performance of the proposed method and four methods based on DL on the entire dataset in terms of six metrics. It can be observed from Table 4 that: (i) the proposed fusion method achieves the best value in terms of three metrics, namely the Qabf, FMI and SCD; (ii) the proposed fusion method achieves the next-best value in terms of the MI and SD; (iii) the proposed fusion method achieves a high value in terms of the MS_SSIM.

In Fig. 9, we also present the images fused by the proposed method using twelve pairs of multi-modality medical images in the dataset.

It is important to note that the proposed fusion method is a NSCT-based method, where DTNP systems are used to improve

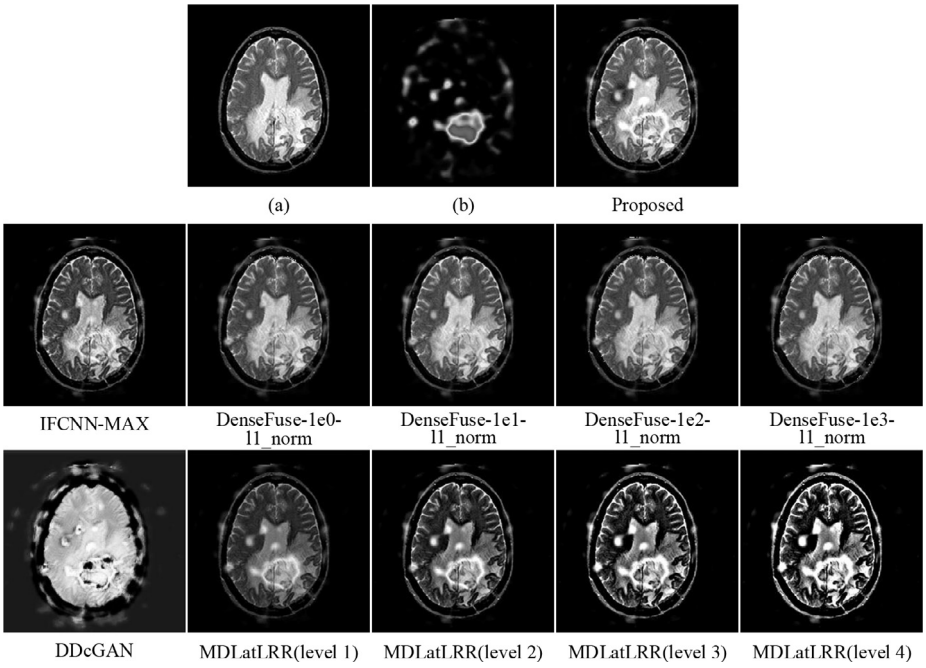

Fig. 8. Fusion results on the 'Group 12' images: (a) source MRI image and (b) source SPECT image.

Table 3
Comparison between the results of the proposed method and fusion methods based on DL on two multi-modality medical images in terms of six metrics.

Images	Method		Qabf	MI	FMI	SCD	MS_SSIM	SD
Group 11	IFCNN-Max		0.5845	8.4333	0.8513	1.3514	0.9395	65.0031
MRI/PET	DenseFuse	$\lambda = 1e^0$	0.5147	8.4868	0.8490	1.1832	0.9108	62.9332
	l_1-norm	$\lambda = 1e^1$	0.5223	8.5148	0.8507	1.2212	0.9073	64.2405
		$\lambda = 1e^2$	0.5140	8.4969	0.8501	1.2012	0.9123	63.2758
		$\lambda = 1e^3$	0.4973	8.5058	0.8440	1.1741	0.8998	64.7645
	DDcGAN		0.1556	**10.0066**	0.7863	1.2004	0.7514	77.2907
	MDLatLRR	level 1	0.5233	8.3320	0.8602	1.0607	0.9363	54.8943
		level 2	**0.6185**	7.8842	0.8584	1.3508	**0.9456**	63.1007
		level 3	0.5413	6.9550	0.8395	1.3437	0.9035	72.5770
		level 4	0.4235	5.9628	0.8233	1.2698	0.8634	**79.6922**
	Proposed		0.6176	9.7471	**0.8621**	**1.5261**	0.9297	72.6617
Group 12	IFCNN-Max		0.6757	8.3005	0.8603	1.1393	0.9569	59.2958
MRI/SPEC	DenseFuse	$\lambda = 1e^0$	0.6751	8.5757	0.8711	0.9672	0.9288	60.4715
	l_1-norm	$\lambda = 1e^1$	0.6865	8.6748	0.8737	0.9777	0.9241	63.1825
		$\lambda = 1e^2$	0.6685	8.6550	0.8692	0.9673	0.9257	60.9806
		$\lambda = 1e^3$	0.6637	8.6017	0.8669	0.9688	0.9233	62.0675
	DDcGAN		0.1003	**11.1360**	0.8308	0.7138	0.5482	**76.3385**
	MDLatLRR	level 1	0.6172	8.0978	0.8759	0.9497	0.9418	45.6005
		level 2	0.6966	7.6814	0.8650	1.0503	**0.9702**	52.8385
		level 3	0.5767	7.1560	0.8510	1.0832	0.9276	62.2445
		level 4	0.4073	6.5555	0.8354	1.0673	0.8718	70.5927
	Proposed		**0.6992**	8.9643	**0.8843**	**1.4128**	0.9607	69.1982

Table 4
Comparison between the results of the proposed method and DL-based methods on the dataset in terms of six metrics.

Images	Method		Qabf	MI	FMI	SCD	MS_SSIM	SD
Dataset	IFCNN-Max		0.5695	10.4741	0.8651	1.1999	0.9342	67.6995
	DenseFuse	$\lambda = 1e^0$	0.5467	10.3444	0.8744	1.0146	0.8933	64.7813
	l_1-norm	$\lambda = 1e^1$	0.5566	10.4553	0.8756	1.0307	0.8911	66.1080
		$\lambda = 1e^2$	0.5465	10.4082	0.8746	1.0162	0.8930	64.9892
		$\lambda = 1e^3$	0.5488	10.3720	0.8737	1.0237	0.8895	66.1107
	DDcGAN		0.2719	**12.0227**	0.8255	1.2149	0.6916	**82.8303**
	MDLatLRR	level 1	0.4799	10.1511	0.8728	0.8861	0.8999	55.0373
		level 2	0.5704	9.9505	0.8703	1.0820	**0.9476**	63.0853
		level 3	0.5136	9.5233	0.8601	1.1752	0.9274	72.8156
		level 4	0.4031	8.9957	0.8453	1.1984	0.8824	80.8270
	Proposed		**0.5805**	11.3653	**0.8787**	**1.4144**	0.9324	75.1189

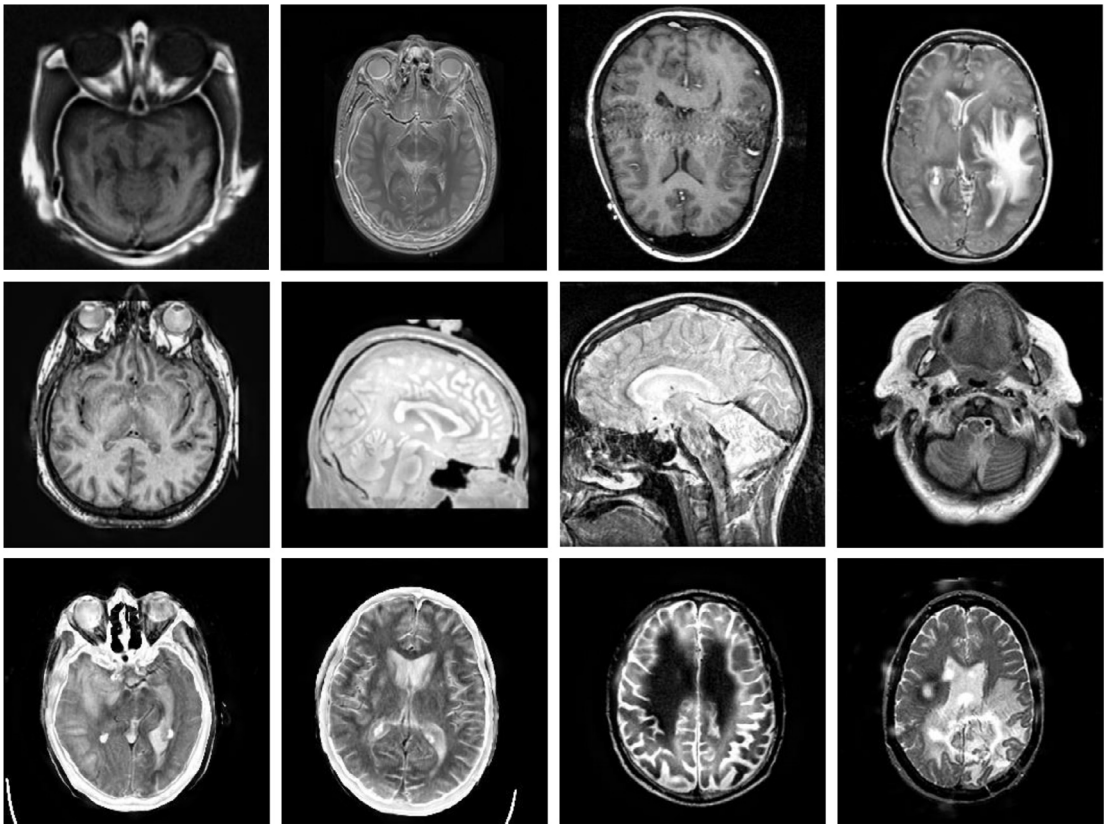

Fig. 9. Fusion results of the proposed method on twelve pairs of multi-modality medical images in the dataset.

its fusion performance. In the experiments, three previously proposed NSCT-based methods, namely the NSCT [22], NSCT-SR [58], NSCT-SF-PCNN [59], were used for comparisons with the proposed method (NSCT+DTNP). Figs. 5 and 6 show that the proposed method achieves better fusion performance. It can be observed from Tables 1 and 2 that the proposed method performs better than the NSCT, NSCT-SR and NSCT-SF-PCNN in terms of a majority of the six evaluated metrics. Moreover, a comparison of the results presented in Tables 3 and 4 indicates that the proposed fusion method can approach or even partially exceed the performance of the four DL-based fusion methods in terms of some metrics. The subjective and objective comparison results demonstrate the superiority of the DTNP systems in improving the performance of the NSCT-based fusion methods.

5. Conclusions

DTNP systems are a type of Turing-universal, distributed parallel computing models. This paper investigated a DTNP system based fusion framework in the NSCT domain for multi-modality medical images. The proposed fusion framework combined the DTNP+NSCT+INSML+WLE features. For the low-frequency NSCT coefficients, the INSML and WLE features are combined to express the main energy and partial details of the multi-modality medical images and develop a fusion rule. For the high-frequency NSCT coefficients, the INSML feature is used to extract the detailed information of the medical images, such as edges and contours, and it is regarded as an external input of the DTNP systems. The INSML features can trigger the spiking of neurons better due to the cooperative spiking mechanism of neurons in DTNP systems. The proposed fusion method was compared with nine previously reported methods and two fusion methods based on DL using twelve pairs of multi-modality medical images in terms of six metrics. The subjective and objective comparison results of the experiments demonstrated the advantages of the proposed fusion method for multi-modality medical images.

The proposed fusion framework employs the combination of the DTNP+NSCT+INSML+WLE for the fusion of multi-modality medical images. This is a limitation of this framework. Owing to the different imaging principles, the complementary information of other types of images, for e.g., multi-focus images, might not be well extracted by the INSML features. Furthermore, this combination may not be suitable for processing other types of images such as infrared and visible images. Therefore, DTNP systems may need to use the proposed combination with other features. Further work will focus on the fusion of other types of images.

In recent years, colour and 3D medical images have received considerable attention. However, the proposed fusion framework is designed relatively for grayscale medical images. Therefore, the fusion framework incorporating the DTNP+NSCT+INSML+WLE cannot be directly applied to colour and 3D medical images. Future studies will focus on developing a framework based on the combination of DTNP+other components for the fusion of colour and 3D medical images.

Declaration of Competing Interest

The authors declare that they have no known competing financial interests or personal relationships that could have appeared to influence the work reported in this paper.

CRediT authorship contribution statement

Bo Li: Conceptualization, Software, Writing - original draft. **Hong Peng:** Conceptualization, Software, Writing - original draft. **Jun Wang:** Conceptualization, Writing - original draft.

Acknowledgment

The authors thank the anonymous reviewers for providing very insightful and constructive suggestions, which have greatly help improve the presentation of this paper.

This work was partially supported by the Research Fund of Sichuan Science and Technology Project (No. 2018JY0083), Research Foundation of the Education Department of Sichuan province (No. 17TD0034), China.

References

[1] S. Li, X. Kang, L. Fang, J. Hu, H. Yin, Pixel-level image fusion: a survey of the state of the art, Inf. Fusion 33 (2017) 100–112.
[2] J. Ma, Y. Ma, C. Li, Infrared and visible image fusion methods and applications: a survey, Inf. Fusion 45 (2019) 153–178.
[3] A.P. James, B.V. Dasarathy, Medical image fusion: a survey of the state of the art, Inf. Fusion 19 (2014) 4–19.
[4] W. Liu, Z. Wang, A novel multi-focus image fusion method using multiscale shearing non-local guided averaging filter, Signal Process. 166 (2020) 1–24. 107252
[5] Y. Liang, Y. Mao, Z. Tang, M. Yan, Y. Zhao, J. Liu, Efficient misalignment-robust multi-focus microscopical images fusion, Signal Process. 161 (2019) 111–123.
[6] L. Liu, L. Xu, H. Fang, Infrared and visible image fusion and denoising via l_2 - l_p norm minimization, Signal Process. 172 (2020) 107546. 1–11
[7] Y. Gao, Y. Su, Q. Li, H. Li, J. Li, Single image dehazing via self-constructing image fusion, Signal Process. 167 (2020) 107284. 1–11
[8] H. Xu, Z. Le, J. Jiang, X. Guo, FusionDN: a unified densely connected network for image fusion, in: Proceedings of the Thirty-Fourth AAAI Conference on Artificial Intelligence (AAAI), 34, 2020, pp. 12484–12491.
[9] Q. Zhang, Y. Liu, R.S. Blum, J. Han, D. Tao, Sparse representation based multi-sensor image fusion for multi-focus and multi-modality images: a review, Inf. Fusion 40 (2018) 57–75.
[10] Z. Liu, Y. Chai, H. Yin, J. Zhou, Z. Zhu, A novel multi-focus approach based on image decomposition, Inf. Fusion 35 (2017) 102–116.
[11] Y. Liu, X. Chen, H. Peng, Z. Wang, Multi-focus image fusion with a deep convolutional neural network, Inf. Fusion 36 (2017) 191–207.
[12] H. Peng, J. Wang, M.J. Pérenz-Jiménez, A. Riscos-Núñez, Dynamic threshold neural p systems, Knowl.-Based Syst. 163 (2019) 875–884.
[13] B. Li, H. Peng, J. Wang, X. Huang, Multi-focus image fusion based on dynamic threshold neural P systems and surfacelet transform, Knowledge-Based Systems 196 (2020) 105794. 1–12
[14] A. Toe, Image fusion by a ratio of low-pass pyramid, Pattern Recognit. Lett. 9 (1989) 245–253.
[15] V.S. Petrovic, C.S. Xydeas, Gradient-based multiresolution image fusion, IEEE Trans. Image Process. 13 (2) (2004) 228–237.
[16] P. Zeeuw, Wavelets and Image Fusion, CWI Amsterdam, 1998.
[17] R. Redondo, F. Šroubek, S. Fischer, G. Cristóbal, Multifocus image fusion using the log-Gabor transform and a multisize windows technique, Inf. Fusion 10 (2) (2009) 163–171.
[18] J.J. Lewis, R.J. OCallaghan, S.G. Nikolov, D.R. Bull, N. Canagarajah, Pixel- and region-based image fusion with complex wavelets, Inf. Fusion 8 (2) (2007) 119–130.
[19] F. Nencini, A. Garzelli, S. Baronti, L. Alparone, Remote sensing image fusion using the curvelet transform, Inf. Fusion 8 (2007) 143–156.
[20] B. Zhang, C. Zhang, Y. Liu, J. Wu, H. Liu, Multi-focus image fusion algorithm based on compound PCNN in surfacelet domain, Optik 125 (2014) 296–300.
[21] X. Jin, G. Chen, J. Hou, Q. Jiang, D. Zhou, S. Yao, Multimodal sensor medical image fusion based on nonsubsampled shearlet transform and s-PCNNs in HSV space, Signal Process. 153 (2018) 379–395.
[22] Q. Zhang, B. Guo, Multifocus image fusion using the nonsubsampled contourlet transform, Signal Process. 89 (7) (2009) 1334–1346.
[23] R. Singh, A. Khare, Fusion of multimodal medical images using Daubechies complex wavelet transform - a multiresolution approach, Inf. Fusion 19 (2014) 49–60.
[24] M. Manchanda, R. Sharma, A novel method of multimodal medical image fusion using fuzzy transform, J. Vis. Commun. Image Represent. 40 (2016) 197–217.
[25] M. Manchanda, R. Sharma, An improved multimodal medical image fusion algorithm based on fuzzy transform, J. Vis. Commun. Image Represent. 51 (2018) 76–94.
[26] S. Singh, R.S. Anand, Ripplet domain fusion approach for CT and MR medical image information, Biomed. Signal Process. Control 46 (2018) 281–292.
[27] K. Padmavathi, C.S. Asha, M.V. Karki, A novel medical image fusion by combining TV-l1 decomposed textures based on adaptive weighting scheme, Engineering Science and Technology (2019). Available at https://doi.org/10.1016/j.jestch.2019.03.008
[28] L. Yang, B. Guo, W. Ni, Multimodality medical image fusion based on multiscale geometric analysis of contourlet transform, Neurocomputing 72 (1-3) (2008) 203–211.
[29] Z. Zhu, H. Yin, Y. Chai, Y. Li, G. Qi, A novel multi-modality image method based on image decomposition and sparse representation, Inf. Sci. 432 (2018) 516–529.
[30] Q. Zhang, T. Shi, F. Wang, R.S. Blum, J. Han, Robust sparse representation based multi-focus image fusion with dictionary construction and local spatial consistency, Pattern Recognit. 83 (2018) 299–313.
[31] X. Ma, S. Hu, S. Liu, J. Fang, S. Xu, Multi-focus image fusion based on joint sparse representation and optimum theory, Signal Process. Image Commun. 78 (2019) 125–134.
[32] M. Zhang, S. Li, F. Yu, X. Tian, Image fusion employing adaptive spectral-spatial gradient sparse regularization in UAV remote sensing, Signal Process. 170 (2020) 1–13. 107434
[33] Y. Zhang, M. Yang, N. Li, Z. Yu, Analysis-synthesis dictionary pair learning and patch saliency measure for image fusion, Signal Process. 167 (2020) 107327. 1–13
[34] Q. Hu, S. Hu, F. Zhang, Multi-modality medical image fusion based on separable dictionary learning and Gabor filtering, Signal Process. Image Communication 83 (2020) 115758. 1–10
[35] H. Li, Y. Wang, Z. Yang, et al., Discriminative dictionary learning-based multiple component decomposition for detail-preserving noisy image fusion, IEEE Trans. Instrum.Meas. 69 (4) (2020) 1082–1102.
[36] Z. Zhu, Y. Chai, H. Yin, Y. Li, Z. Liu, A novel dictionary learning approach for multi-modality medical image fusion, Neurocomputing 214 (2016) 471–482.
[37] H. Li, X. He, D. Tao, Y. Tang, R. Wang, Joint medical image fusion, denoising and enhancement via discriminative low-rank sparse dictionaries learning, Pattern Recognit. 79 (2018) 130–146.
[38] Y. Liu, X. Chen, R.K. Ward, Z. Wang, Medical image fusion via convolutional sparsity based morphological component analysis, IEEE Signal Process. Lett. 26 (3) (2019) 485–489.
[39] Q. Hu, S. Hu, F. Zhang, Multi-modality medical image fusion based on separable dictionary learning and Gabor filtering, Signal Process.: Image Communication 83 (2020) 115758. 1–10
[40] Y. Jiang, M. Wang, Image fusion with morphological component analysis, Inf. Fusion 18 (7) (2014) 107–118.
[41] Z. Xu, Medical image fusion using multi-level local extrema, Inf. Fusion 19 (11) (2014) 38–48.
[42] S. Maqsood, U. Javed, Multi-modal medical image fusion based on two-scale image decomposition and sparse representation, Biomed. Signal Process. Control 57 (2020) 101810.
[43] H. Tang, B. Xiao, W. Li, G. Wang, Pixel convolutional neural network for multi-focus image fusion, Inf. Sci. 433 (2017) 125–141.
[44] X. Gao, R. Nie, J. Cao, D. Zhou, W. Qian, Fully convolutional network-based multi-focus image fusion, Neural Comput. 30 (7) (2018) 1775–1800.
[45] M. Amin-Naji, A. Aghagolzadeh, M. Ezoji, Ensemble of CNN for multi-focus image fusion, Inf. Fusion 51 (2019) 201–214.
[46] H. Li, X. Wu, DenseFuse: a fusion approach to infrared and visible images, IEEE Trans. Image Process. 28 (5) (2019) 2614–2623.
[47] Y. Zhang, Y. Liu, IFCNN: a general image fusion framework based on convolutional neural network, Inf. Fusion 54 (2020) 99–118.
[48] J. Ma, H. Xu, J. Jiang, X. Mei, X. Zhang, DDcGAN: a dual-discriminator conditional generative adversarial network for multi-resolution image fusion, IEEE Trans. Image Process. 29 (2020) 4980–4995.
[49] H. Li, X. Wu, J. Kittler, MDLatLRR: a novel decomposition method for infrared and visible image fusion, IEEE Transactions on Image Processing (2020). Available at https://doi.org/10.1109/TIP.2020.2975984.
[50] M. Ionescu, G. Păun, T. Yokomori, Spiking neural P systems, Fundamenta Informaticae 71 (2006) 279–308.
[51] H. Peng, J. Yang, J. Wang, T. Wang, Z. Sun, X. Song, X. Luo, X. Huang, Spiking neural P systems with multiple channels, Neural Netw. 95 (2017) 66–71.
[52] H. Peng, J. Wang, Coupled neural P systems, IEEE Trans. Neural Netw. Learn.Syst. 30 (6) (2019) 1672–1682.
[53] H. Peng, B. Li, J. Wang, X. Song, T. Wang, L. Valencia-Cabrera, I. Pérez-Hurtado, A. Riscos-Núñez, M.J. Pérenz-Jiménez, Spiking neural P systems with inhibitory rules, Knowledge-Based Systems 188 (2020) 105064. 1–10
[54] H. Peng, Z. Lv, B. Li, X. Luo, J. Wang, X. Song, T. Wang, M.J. Pérenz-Jiménez, A. Riscos-Núñez, Nonlinear spiking neural P systems, International Journal of Neural Systems (2020). Available at https://doi.org/10.1142/S0129065720500082.
[55] H. Peng, T. Bao, X. Luo, J. Wang, X. Song, A. Riscos-Núñez, M.J. Pérenz-Jiménez, Dendrite P systems, Neural Netw. 127 (2020) 110–120.
[56] X. Li, X. Tian, Y. Sun, Z. Tang, Medical image fusion by multi-resolution analysis of wavelets transform, in: Wavelet Analysis and Applications, Applied and Numerical Harmonic Analysis, 2007, pp. 389–396.
[57] Y. Y. Liu, Z. Wang, Simultaneous image fusion and denoising with adaptive sparse representation, IET Image Process. 9 (5) (2015) 347–357.
[58] Y. Liu, S. Liu, Z. Wang, A general framework for image fusion based on multi-scale transform and sparse representation, Inf. Fusion 24 (2015) 147–164.

[59] X. Qu, J. Yan, H. Xiao, Z. Zhu, Image fusion algorithm based on spatial frequency-motivated pulse coupled neural networks in nonsubsampled contourlet transform domain, Acta Autom. Sin. 34 (12) (2008) 1508–1514.
[60] M. Yin, X. Liu, Y. Liu, X. Chen, Medical image fusion with parameter-adaptive pulse coupled-neural network in nonsubsampled shearlet transform domain, IEEE Trans. Instrum. Meas. 68 (1) (2018) 49–64.
[61] C. Xydeas, V. Petrovic, Objective image fusion performance measure, Electron. Lett. 36 (4) (2009) 308–309.
[62] G. Qu, D. Zhang, P. Yan, Information measure for performance of image fusion, Electron. Lett. 38 (7) (2002) 313–315.
[63] M.B.A. Haghighat, A. Aghagolzadeh, H. Seyedarabi, A non-reference image fusion metric based on mutual information of image features, Comput. Electr. Eng. 37 (5) (2011) 744–756.
[64] V. Aslantas, E. Bendes, A new image quality metric for image fusion: the sum of the correlations of differences, AEU Int. J. Electron.Commun. 69 (12) (2015) 1890–1896.
[65] K. Ma, K. Zeng, Z. Wang, Perceptual quality assessment for multi-exposure image fusion, IEEE Trans. Image Process. 24 (11) (2015) 3345–3356.
[66] M. Deshmukh, U. Bhosale, Image fusion and image quality assessment of fused images, Int. J. Signal Process. Image Process. Pattern Recognit. 4 (2010) 484–508.